



# Simultaneous radio and optical observations of the mid-latitude atmospheric response to a major geomagnetic storm of 6–8 April 2000

E.L. Afraimovich<sup>a,\*</sup>, Ya.F. Ashkaliev<sup>b</sup>, V.M. Aushev<sup>b</sup>, A.B. Beletsky<sup>a</sup>,  
V.V. Vodyannikov<sup>b</sup>, L.A. Leonovich<sup>a</sup>, O.S. Lesyuta<sup>a</sup>, Yu.V. Lipko<sup>a</sup>, A.V. Mikhalev<sup>a</sup>,  
A.F. Yakovets<sup>b</sup>

<sup>a</sup>*Institute of Solar-Terrestrial Physics, Russian Academy of Sciences, P.O. Box, 4026, 664033 Irkutsk, Russia*

<sup>b</sup>*Institute of Ionosphere, Almaty 480020, Kazakhstan*

Received 8 August 2001; received in revised form 11 April 2002; accepted 5 July 2002

## Abstract

Basic properties of the mid-latitude traveling ionospheric disturbances (TIDs) during the maximum phase of a major magnetic storm of 6–8 April 2000 are shown. Total electron content (TEC) variations were studied by using data from GPS receivers located in Russia and Central Asia. The nightglow response to this storm at mesopause and thermospheric altitudes was also measured by optical instruments FENIX located at the observatory of the Institute of Solar-Terrestrial Physics (51.9°N, 103.0°E), and MORTI located at the observatory of the Institute of Ionosphere (43.2°N, 77.0°E). Observations of the O (557.7 and 630.0 nm) emissions originating from atmospheric layers centered at altitudes of 90 and 250 km were carried out at Irkutsk and of the O<sub>2</sub>(b<sup>1</sup>Σ<sub>g</sub><sup>+</sup>–X<sup>3</sup>Σ<sub>g</sub><sup>-</sup>) (0-1) emission originating from an atmospheric layer centered at altitude of 94 km was carried out at Almaty. Our radio and optical measurement network observed a storm-induced solitary large-scale wave with duration of 1 h and a wave front width of no less than 5000 km, while it traveled equatorward with a velocity of 200 m/s from 62°N to 38°N geographic latitude. The TEC disturbance, basically displaying an electron content depression in the maximum of the F2 region, reveals a good correlation with growing nightglow emission, the temporal shift between the TEC and emission variation maxima being different for different altitudes. A comparison of the auroral oval parameters with dynamic spectra of TEC variations and optical 630 nm emissions in the frequency range 0.4–4 mHz (250–2500 s periods) showed that as the auroral oval expands into mid-latitudes, also does the region with a developed medium-scale and small-scale TEC structure.

© 2002 Elsevier Science Ltd. All rights reserved.

**Keywords:** Geomagnetic storm; Traveling ionospheric disturbances; Optical emission; Total electron content; GPS

## 1. Introduction

In the course of major geomagnetic storms, significant changes in main structural elements of the magnetosphere and ionosphere occur. Geophysical manifestations of major

magnetic storms are of particular interest because these storms take place relatively rarely (no more than 4 events during an 11-year solar cycle), and therefore the representative statistics of the whole complex of interactive processes in the “magnetosphere–ionosphere” system is lacking.

Although the term “major magnetic storm” is a rather arbitrary designation for magnetic storms with a maximum  $D_{st}$ -deviation exceeding 100–200 nT, it is more frequently used than the “large” or “strong” magnetic storm (in, for

\* Corresponding author. Fax: +7-3952-462557.

E-mail address: [afr@iszf.irk.ru](mailto:afr@iszf.irk.ru) (E.L. Afraimovich).

example, a paper of Ho et al. (1998)). There is no question that the 6 April 2000 magnetic storm refers to the strongest storms (see Section 2); hence the term “major magnetic storm” will be used to designate this storm throughout the text.

We have now reached a new quality level in studying these phenomena because a large number of ionospheric and magnetospheric parameters are continuously monitored by various ground-based and space facilities. A new era in the remote ionospheric monitoring was opened up with the advent of the Global Positioning System (GPS) now comprising more than 900 world-wide two-frequency GPS receivers whose data are available through the Internet.

Large-scale traveling ionospheric disturbances (LS TIDs) with a period of 1–2 h and a wavelength of 1000–2000 km constitute the most significant mid-latitude consequence of magnetic storms. Many papers including review papers (Hunsucker, 1982; Hocke and Schlegel, 1996) have been published. LS TIDs are considered to be a manifestation of internal atmospheric gravity waves (AGWs) excited by sources in the polar regions of the northern and southern hemispheres. Thus, the study of LS TIDs provides important information on auroral processes under quiet and disturbed geomagnetic conditions.

Afraimovich et al. (2000) were the first to develop a technique for determining the LS TIDs parameters based on calculations of spatial and temporal gradients of total electron content (TEC) measured by three spaced GPS receivers (a GPS array). This technique was employed to determine the LS TIDs parameters in the course of a major magnetic storm of 25 September 1998. It was shown that a large-scale solitary wave excited in the auroral region with a duration of about 1 h and the front width of 3700 km, at least, traveled equatorward to a distance no less than 2000–3000 km with the average velocity of about 300 m/s.

Another interesting consequence of major magnetic storms is low-latitude auroras. The global response to the magnetic storm of the year 1989 was studied by Yeh et al. (1994). Low-latitude auroras were observed in the northern and southern hemispheres. A long-term electron density depression in the mid-latitude ionosphere is the most pronounced effect of the storm (Buonsanto, 1999). During the maximum phase of the storm, the zone of disturbances extended to geomagnetic latitudes of less than  $10^\circ$  causing a temporal depression of the equatorial anomaly.

There appeared many papers on the behavior of night-glow emissions of the upper atmosphere (Chapman, 1957; Ishimoto et al., 1986; Tinsley, 1979; Torr and Torr, 1984). Several peculiarities in spectra of upper atmosphere emissions at the middle and low latitudes during strong geomagnetic perturbations allow them to be classified as “mid- and low-latitude auroras” (Rassoul et al., 1993) distinguishing from the “common” aurora at polar latitudes. The differences between auroras include the appearance of the  $N_2^+$  emission in bands of the first negative system of mid-latitude spectra, a significant increase of the atomic oxygen (630.0 nm)

emission, and the predominance of emissions of atomic ion lines above these of molecular bands.

Rassoul et al. (1993) classified several types of low-latitude auroras in relation to the type of bombarding particles (electrons, ions, neutral particles), dominating emissions, localization, and typical temporal scales. Many observations revealed several types of simultaneously existing auroras caused by the bombardment of fast electrons and mixture heavy particles. At mid-latitudes during moderate geomagnetic perturbations, 630 nm emission variations with periods ranging from 0.5 to 2 h were recorded (Misawa et al., 1984; Sahal et al., 1988). Mid-latitude auroras occurring in the course of very major magnetic storms ( $K_p \geq 8$ ,  $D_{st} \leq -300$  nT) are of the particular interest because the number of observations with optical instruments was limited.

Although mid-latitude ionospheric storms have been studied during several decades, there is no complete explanation of their effects because of the small number of sounding facilities and their low spatial and temporal resolutions of an ionosonde, an incoherent scatter radar and optical devices. Moreover, in contrast to polar latitudes, a small number of observations were carried out at mid-latitudes simultaneously by radio and optical techniques which supplement each other because they allow their shortcomings to be compensated and the reliability of interpretation of phenomena to be increased.

The objective of this paper is to study the response of the mid-latitude ionosphere to the major magnetic storm of 6 April 2000 by using data of simultaneous radio and optical observations in Russia and Central Asia, main attention being paid to LS TIDs with a characteristic temporal period on the order of 1 h and to medium- and small-scale disturbance, whose increase in intensity is related to the shift of the auroral region toward mid-latitudes.

Section 2 gives a description of the state of the geomagnetic field on 6–7 April 2000, and the scheme of the experiment. The features of LS TIDs obtained on the basis of TEC and optical and ionosonde data are described in Sections 3 and 4. Section 5 compares the auroral oval parameters with dynamic spectra of TEC variations and optical 630 nm emissions in the frequency range 0.4–4 MHz (250–2500 s periods). Section 6 is devoted to the discussion of the results.

## 2. Description of the state of the geomagnetic field in 6–7 April 2000, and scheme of the experiment

Fig. 1 shows the  $K$ -index (a), the  $D_{st}$  variations of the geomagnetic field, and the variations of the  $H$ -component of the geomagnetic field at Almaty (c) and Irkutsk (g) in the course of the major magnetic storm of 6–8 April 2000. This storm was characterized by a pronounced sudden commencement (SSC) that started at 16:42 UT. At the maximum of the storm, the  $K$ -index achieved the value 8, and a

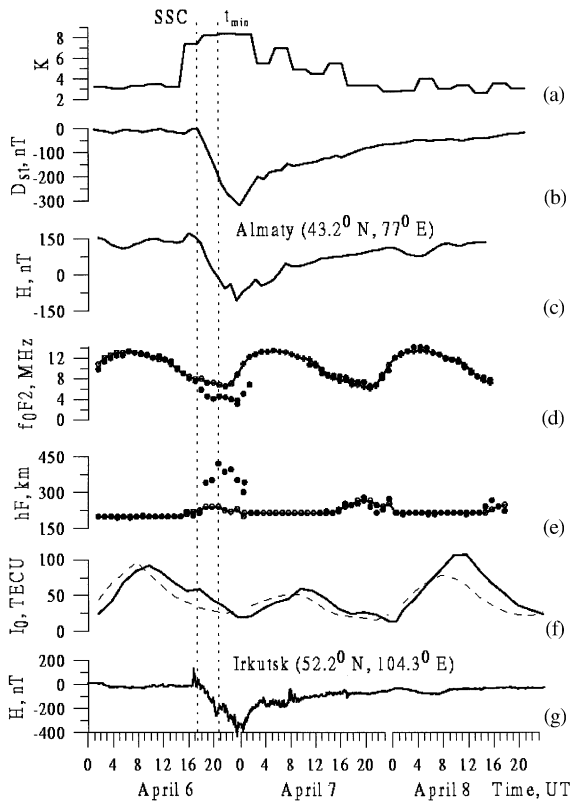


Fig. 1.  $K$ -index (a),  $D_{st}$ -variations of the geomagnetic field (b), variations of the  $H$ -component of the geomagnetic field at Almaty (c), and at Irkutsk (g) during the major magnetic storm of 6–8 April 2000. Variations of the critical frequency  $f_0F_2$  (d) and virtual height  $hF$  of the F2-layer (e) at Almaty (heavy dots); current median meanings of these parameters are plotted by solid lines. Variations of the absolute vertical value of TEC  $I_0(t)$  for the same time interval at Almaty (solid line) and at Irkutsk (dashed line) (f). Dashed vertical lines denote moments of SSC and  $t_{min}$ , the interval inside these moments being corresponded the maximum value of  $dD_{st}/dt$ .

$K$ -index diurnal sum of 48 was observed. At 16:00 UT on 6 April, the  $D_{st}$  amplitude increased fast to 0, but after that it began to decrease, and at 24:00 UT it reached the value  $-319$  nT. After that, the recovery phase continued into 8 April. In Fig. 1, the dashed vertical lines show SSC and  $t_{min} = 20:00$  UT corresponding to the maximum value of the time derivative of  $D_{st}$  ( $dD_{st}/dt$ ).

Fig. 2 shows the scheme of the experiment in the geographical system of coordinates. The positions of the GPS receivers are denoted by heavy dots, and their names are given. On the upper scale, the values of the local time (LT) for a certain longitudinal interval corresponding to the relative time of the arrival of the LS TID at middle latitudes at 19:00 UT are plotted (Section 3). Diamonds and slant letters show the positions of optical instruments MORTI (near Almaty and station SELE) and FENIX (near Irkutsk and station IRKT).

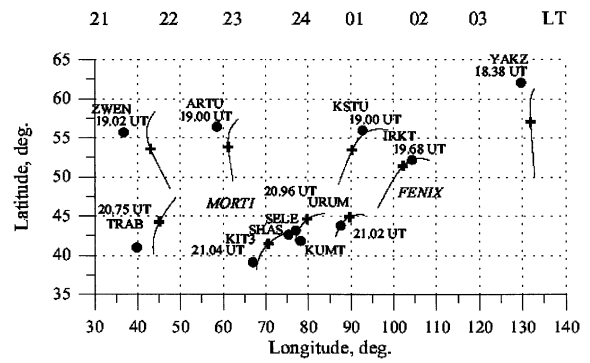


Fig. 2. A scheme of the experiment in the geographical system of coordinates. Positions of GPS receivers are denoted with heavy dots and their names are placed there. Solid lines represent trajectories of subionospheric points motion for the satellite PRN25 at the altitude of 400 km. Crosses at the trajectories denote positions of subionospheric points at moments  $t_{min}$  when minimum TEC occurs (see Figs. 3 and 4);  $t_{min}$  expressed in decimals of an hour (UT). On the upper scale, values of a local time (LT) for the certain longitude interval corresponding to the relative time of the arrival of the LS TID in middle latitudes at 19:00 UT are plotted (Section 3). Diamonds and slant letter show positions of optical instruments MORTI (near Almaty and station SELE) and FENIX (near Irkutsk and station IRKT).

Almaty and station SELE) and FENIX (near Irkutsk and station IRKT). Data of an Almaty standard ionosonde were also used in this paper.

GPS receivers are distributed all over the world with a different density, and the region considered in this paper comprises only 11 stations whose coordinates are listed in Table 1. Parameters of LS TIDs are considered to have been determined with a proper reliability when the distances between GPS receivers exceed the wavelength of TIDs (about 1000 km). The array of GPS receivers used in the experiment satisfied this requirement.

### 3. Parameters of LS TIDs measured by GPS receivers and the Almaty ionosonde

The GPS technique makes it possible to determine the parameters of TIDs from the phase variations at two carrier frequencies measured at spaced sites. Methods of calculating the relative slant TEC variations  $I_S$  from measurements of the ionosphere-induced change in the phase path of GPS signals were described in detail in several papers (Hofmann-Wellenhof et al., 1992; Afraimovich et al., 1998, 2000). Here we reproduce the resulting expression for phase measurements:

$$I_S = \frac{1}{40.308} \frac{f_1^2 f_2^2}{f_1^2 - f_2^2} [(\varphi_1 \lambda_1 - \varphi_2 \lambda_2) + const + nL], \quad (1)$$

Table 1  
GPS site and optical instrument names and locations

No.	Instrument	Latitude°N	Longitude°E	$t_{\min}$ , UT	$A_{\min}$ , TECU
1	YAKZ	62.031	129.681	18.383	−4.55
2	ARTU	56.430	58.560	19.000	−4.94
3	KSTU	55.993	92.794	19.000	−3.78
4	ZWEN	55.699	36.759	19.025	−0.95
5	IRKT	52.219	104.316	19.683	−2.28
6	URUM	43.808	87.601	21.017	−0.81
7	SELE	43.179	77.017	20.958	−0.71
8	SHAS	42.621	75.315	20.925	−0.69
9	KUMT	41.863	78.190	20.992	−0.91
10	TRAB	40.995	39.775	20.750	−1.47
11	KIT3	39.135	66.885	21.042	−0.61
12	FENIX	51.9	103.0		
13	MORTI	43.05	76.97		

where  $\varphi_1\lambda_1$  and  $\varphi_2\lambda_2$  are additional phase paths of radio signals caused by phase delays in the ionosphere (m);  $\varphi_1$  and  $\varphi_2$  represent the number of phase rotations, and  $\lambda_1$  and  $\lambda_2$  are the wavelengths at frequencies  $f_1 = 1575.42$  and  $f_2 = 1227.6$  MHz; *const* is some unknown initial phase path (m); and  $nL$  is the error in determining the phase path (m).

For this type of measurements with the sampling rate of 30 s, the error of TEC measurements does not exceed  $10^{14} \text{ m}^{-2}$ , the initial value of TEC being unknown (Hofmann-Wellenhof et al., 1992). This makes it possible to detect irregularities and waves in the ionosphere over a wide band of amplitudes (up to  $10^{-4}$  of the diurnal TEC variation) and periods (more than 5 min). The TEC unit (TECU), which is equal to  $10^{16} \text{ m}^{-2}$  and commonly, accepted in the art, will be used in the following.

There exist different methods for reconstructing TEC series, the length of which far exceeds the duration of continuous observations from one of the GPS satellites at elevations exceeding our specified threshold of  $30^\circ$  (no more than 4–6 h). However, to do this requires invoking data of phase measurements for all GPS satellites that are visible for 24 h, remove the ambiguity of these measurements and reconstruct long TEC series on the basis of some electron density distribution model.

Initial data to calculate the parameters of TEC variations were time-series of TEC at certain sites with corresponding time-series of the angle of elevation  $\theta(t)$  and azimuth  $\alpha(t)$  for the satellite-receiver line calculated by using software CONVTEC which was able to interpret GPS RINEX-files. Continuous time-series of  $I_S(t)$  measurements with a duration no less than 3 h were chosen for determining the LS TIDs parameters.

To exclude trends caused by regular changes in ionospheric density and satellite motion, an hour running average was subtracted from the TEC time-series.  $\theta(t)$  and  $\alpha(t)$  were employed to calculate coordinates of subionospheric points. To convert the variations of slant TEC to that of verti-

cal TEC, the a well-known technique was used (Klobuchar, 1986)

$$I = I_S \cos \left[ \arcsin \left( \frac{R_z}{R_z + h_{\max}} \cos \theta \right) \right], \quad (2)$$

where  $R_z$  is the Earth's radius, and  $h_{\max} = 300$  km is the altitude of the F2 layer maximum.

### 3.1. Parameters of large-scale traveling ionospheric disturbances determined from GPS data

Figs. 3 and 4 show the initial  $I(t)$  and detrended time-series  $dI(t)$  for GPS satellite number PRN25. For the YAKZ site, only data from the PRN30 satellite for the interval 17:00–20:00 UT were available for technical reasons. Almost all GPS records show a gradual decrease of  $I(t)$  till a certain time ( $t_{\min}$ ) corresponding to minima (designated by diamonds in Figs. 3 and 4) in TEC variations,  $t_{\min}$  depending on the latitude of the GPS site. Large fast variations of TEC occur for some sites after  $t_{\min}$  has elapsed.

Satellite PRN25 was chosen for all GPS sites analyzed (except YAKZ) because its minimum elevation angle  $\theta(t)$  exceeded  $45^\circ$  for every station during 19:00–21:00 UT. Thus, the error of converting the slanting TEC to vertical one caused by the difference between the actual and spherically symmetric spatial TEC distributions was minimized.

In Fig. 2, the solid lines show trajectories of motion of subionospheric points for satellite PRN25 (PRN30 for YAKZ) at the altitude of 400 km. Crosses at the trajectories indicate the positions of subionospheric points at  $t_{\min}$  corresponding to minimum TEC (Figs. 3 and 4). Near crosses one can find the value of  $t_{\min}$  expressed in terms of decimal parts of an hour. For the subionospheric point of every GPS station, the values of  $t_{\min}$  and amplitudes ( $A_{\min}$ ) expressed in TECU are listed in Table 1. As is seen from Fig. 2, a minimum  $dI$  was first recorded for the subionospheric point of station YAKZ at  $57^\circ\text{N}$  latitude (thin line in

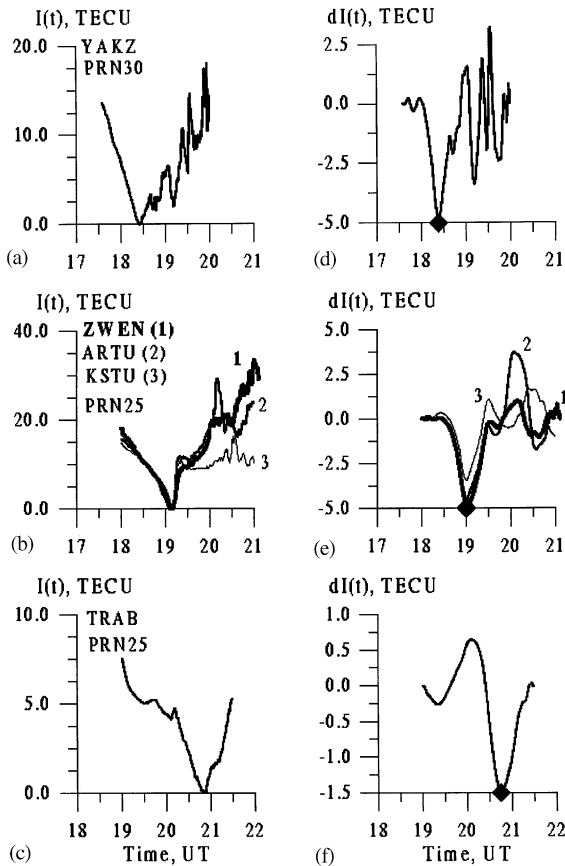


Fig. 3. The initial time-series of slant TEC,  $I(t)$ , at GPS stations ZWEN (very thick line 1), ARTU (thick line 2), KSTU (thin line 3) for satellite PRN25 and 6 April, 2000 (b) and TRAB (c); and detrended ones,  $dI(t)$ , (e), and (f). Panels (a) and (d) represent  $I(t)$  and  $dI(t)$  variations at the station YAKZ for satellite PRN30. Diamonds at temporal axes denote moments,  $t_{\min}$  of minimum  $dI(t)$ .

Fig. 3c), and, after that, almost simultaneously it was recorded near  $53^\circ\text{N}$  latitude at stations ZWEN, ARTU, KSTU (Fig. 3a, d; b, e; c, f, respectively) which are extended along the same parallel over the longitudinal difference of  $47^\circ$ . Clearly, the ionospheric disturbance had a wave front with its length exceeding 5000 km. The same result was obtained by Afraimovich et al. (2000). Forty minutes later this disturbance was recorded at the subionospheric point for station IRKT at  $51.5^\circ\text{N}$  latitude (Fig. 4a and d). Two hours later a similar disturbance  $dI(t)$  was recorded at a chain of stations TRAB, SELE (Fig. 4b and e), KITS, KUMT and URUM (Fig. 4c and f) at  $40^\circ\text{--}45^\circ\text{N}$  latitudes.

By using Table 1 and Figs. 3 and 4, one can study the evolution of the disturbance as it travels equatorward. The amplitude ( $A_{\min}$ ) of the disturbance  $dI(t)$  decreases from 5 TECU at the northern chain of stations to 1 TECU at the southern chain. Moreover, large fast variations  $dI(t)$

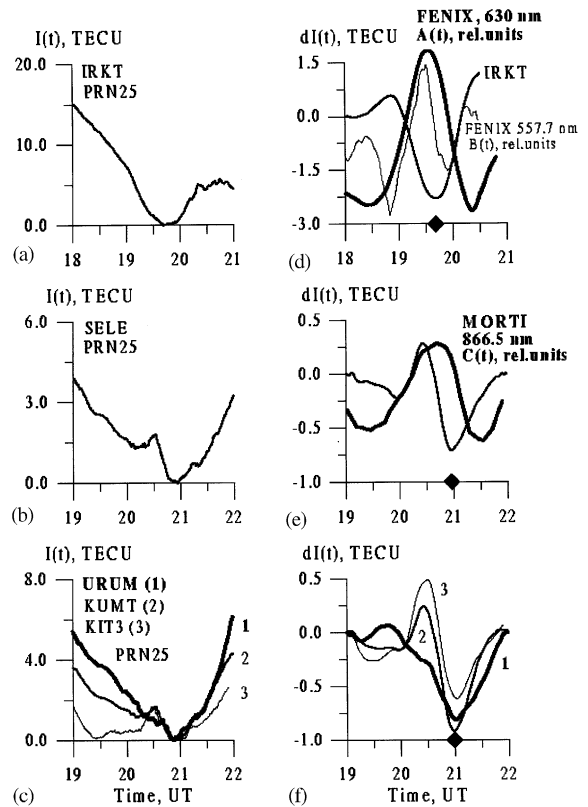


Fig. 4. As in Fig. 3, but for GPS stations IRKT (a; d—thick line), SELE (b; e—thick line), URUM (very thick line 1), KUMT (thick line 2), and KIT3—thin line 3 (c, f). For comparison, very thick line at the panel (d) show behavior of the 630 nm emission rate  $A(t)$  and thin line show the 577.7 nm emission rate  $B(t)$  recorded by the instrument FENIX and filtered from initial data (Fig. 5a, curves 1, 2, respectively), as it was done for TEC data,  $I(t)$ . Behavior of the 866.5 nm emission rate  $C(t)$  recorded by the instrument MORTI and filtered from initial data (Fig. 6b), as it was done for TEC data, presented at the panel (e) by very thick line. Observations of the O (557.7 nm, 630.0 nm) emissions originating from atmospheric layers centered at altitudes of 97 and 250 km were carried out at Irkutsk.

typical of the high-latitude ionosphere were recorded after passing a minimum  $dI(t)$  at the northern chain of stations. These variations are noticeably less at the southern chain of stations.

These features of the  $dI(t)$  variations seem to be accounted for the fact that at about 19:00 UT satellite-receiver lines for the northern chain of stations (Fig. 2) crossed the southern boundary of the auroral zone moving southward. If the front of the disturbance has traveled with a constant velocity, then a delay on the order of 2 h between the times of the rise of the disturbances at the northern and southern chains of stations corresponds to the southward velocity of about 200 m/s.



So, in the main phase of the major magnetic storm, a significant descent on the order of 15–20 TECU was observed at the northern chain of GPS sites, including ZWEN, ARTU, KSTU and YAKZ. By means of a chain of ionosondes, Maeda and Handa (1980) and Whalen (1987) obtained similar results. The extension of the disturbance front on the order of 5000 km obtained in this study is consistent with results reported by Whalen (1987), Hajkowicz and Hunsucker (1987), and Afraimovich et al. (2000). Hunsucker (1982) and Balthazor and Moffett (1999) showed that a large area of the polar atmosphere leaving abruptly the state of equilibrium must become the source of LS TIDs traveling equatorward. It is necessary to point out that this period of time was characterized by a maximum time derivative  $D_{st}$  (Fig. 1c) which is consistent with the conclusion of Ho et al. (1998).

### 3.2. Variations of the critical frequency and virtual altitude of the F2 layer over Almaty

Fig. 1d shows the variations of the critical frequency of the F2 layer ( $f_0F2$ ) (heavy dots). The solid line represents the  $f_0F2$  current median defined from 3-month data (Wrenn et al., 1987). The day before the magnetic storm was magnetically quiet, and  $f_0F2(t)$  was close to its median values. The main phase of the magnetic storm occurred at local night at Almaty. A decrease of  $f_0F2$  relative to the median, reflecting a depression of the electron content in the F2 layer maximum, began soon after the beginning of the storm and a maximum difference between the current  $f_0F2$  and median values took place at the period of a maximum time derivative  $dD_{st}/dt$ . The growth of  $f_0F2$  after the solar ionizing agent appeared is delayed with respect to the median by 2 h. Unfortunately, during 7 h after 02:00 UT the ionosonde did not operate for technical reasons; therefore, the time at which  $f_0F2$  approached median values was uncertain.

Variations of the virtual altitudes  $hF$  are plotted in Fig. 1e with heavy dots. The solid line shows the behavior of the  $hF$  current median. It is seen from Fig. 1e that an abrupt increase of  $hF$  with respect to median values began simultaneously with the decrease of  $f_0F2$ . The approach to the median values occurred at 01:00 UT. At that time  $f_0F2$  was equal to 6.0 MHz, and the median value was 11 MHz. The large decrease of  $f_0F2$  in the course of the main phase of the magnetic storm is consistent with the large negative disturbance of TEC recorded by GPS stations (Fig. 4).

Thus, this magnetic storm was accompanied by a very large decrease of the electron content in the maximum of the F2 layer, and by a significant increase of its virtual altitude.

### 3.3. Variations of the vertical TEC value as deduced from GIM data

Recently a number of authors (Wilson et al., 1995; Mannucci et al., 1998 and others) have developed a new technology for constructing global maps of absolute “vertical” val-

ues of TEC using data from the IGS network (Global Ionospheric Maps—GIM Technology). Coupled with the possibility of obtaining these maps in the standard IONEX format on the Internet, the GIM technology provided researchers with a new powerful tool for studying large-scale ionospheric processes under quiet and disturbed conditions on a global scale. This technology has now been used to obtain such new evidence of the global development of large-scale ionospheric disturbances during major ionospheric storms, which was previously unfeasible with relatively sparse conventional facilities such as ionosondes or even incoherent scatter radars.

The essence of the GIM technology and its implementation is described in an extensive series of publications (Wilson et al., 1995; Mannucci et al., 1998; and others); therefore, a detailed description of them will not be given here for reasons of space. Currently, 2-h TEC maps are available to any user; they are calculated by several research groups in the USA and Europe and posted on the Internet in a standard IONEX format. Where necessary, 15-min maps can also be accessed.

Variations of the absolute vertical value of TEC  $I_0(t)$  during the major magnetic storm of 6–8 April 2000 at Almaty (solid line) and at Irkutsk (dashed line) were presented on Fig. 1f.

A distinguishing feature of the  $I_0(t)$ -dependence is clearly pronounced depression of the daytime TEC maximum the day after the storm onset, making up no more than 60% of the corresponding values for the background days of April 6 and 8. This is consistent with published results obtained on the basis of data from ionospheric stations and TEC measurements using signals from geostationary satellites (Proless et al., 1991; Buonsanto, 1999). Unfortunately, the picture of this phenomenon is incomplete for lack of relevant data from the ionosondes at Irkutsk and Almaty.

## 4. Optical observations of nightglow emission

### 4.1. Large-scale disturbances of nightglow emissions over Irkutsk

An optical facility FENIX is settled at Geophysical observatory attached to Institute of Solar-Terrestrial Physics SD RAS at 100 km from Irkutsk city (51.9°N, 103.0°E; geomagnetic latitude is 41.0°N,  $L=2$ ). It includes a four-channel zenith photometer and a high sensitive TV-system comprising an electron-optical amplifier and a charge coupled device (CCD) array.

Following observations of nightglow emissions were made: the OI (557.7 nm) emission which originates from a layer centered at 97 km and with boundaries at altitudes of 85 and 115 km, the OI (630.0 nm) emission which originates from a layer centered at 250–270 km and with boundaries at altitudes of 160–300 km, the O<sub>2</sub> (360–410 nm) emission which originates from a layer centered at

97 km or  $N^{2+}$  (during geomagnetic disturbances), and the OH emission (720–830 nm) which originates from a layer centered at 85–90 km and with boundaries at altitudes of 75–115 km.

Emission lines of 557.7 and 630 nm were recorded by using narrow band (1–2 nm halfwidth) sweeping interference filters. The angle of view of instruments was about 4–5°. The instruments were absolutely calibrated periodically by using the standard stars and were controlled by using reference lamps in periods between absolute calibrations. The software provided records of the emission rate with an exposure time of 12 s, but when the emission rate exceeded the predetermined level, a shorter exposure time of 8 ms was used. In the course of the magnetic storm of 6 April 2000, the records were taken only by the four-channel zenith photometer.

Variations of the nightglow emission rate, derived from the zenith photometer observations on 6 April 2000, are plotted in Fig. 5a. The main feature of these variations is a significant increase of the OI (630.0 nm) emission in the second half of the night (Fig. 5a, line 1) by a factor of 20 compared with values observed near midnight and the last geomagnetic quiet night of 5 April 2000 (Fig. 5a, line 3). It can be seen that the OI (630.0 nm) emission grew after 16:00 UT till sunrise when the observations were completed, and periodical variations were superimposed on the gradual growth. The OI (557.7) emission variations (Fig. 5a, line 2) revealed a small disturbance near 17:00 UT coinciding with a similar disturbance in the OI (630.0 nm) emission, and an abrupt rise (35%) coinciding with the first phase of the OI (630.0 nm) emission rate maximum increase.

Besides, a gradual increase of the signal in the spectral range 360–410 nm, not typical of the quiet geomagnetic state was observed with superimposed irregular short-period variations, to begin at 17.00 UT. The 720–830 nm emission revealed a gradual decrease from 14.00 to 16.00 UT and ended at 16.00 UT when the commencement of the geomagnetic storm occurred.

It is of interest to compare these data with variations of TEC measured at the nearest GPS station IRKT. Records of the 630 and 577.7 nm emission lines ( $A(t)$  and  $B(t)$ ) filtered out from the initial data (Fig. 5a, lines 1 and 2, respectively) as it was done with TEC  $I(t)$ , are plotted in Fig. 4d. It is seen that there is a good correlation between these variations, and the emission variations are in an opposite phase compared with TEC variations. The possible reasons for this behavior are discussed in part 6.

#### 4.2. Large-scale disturbances observed by the MORTI instrument

The Mesopause Rotational Temperature Imager (MORTI) instrument is installed near Almaty in the mountains at 2800 m above sea level (43.05°N, 76.97°E). MORTI provides information for obtaining the rotational temperature and emission rate of the  $O_2(b^1 \sum_g^+ - X^3 \sum_g^-)$  (0-1) atmo-

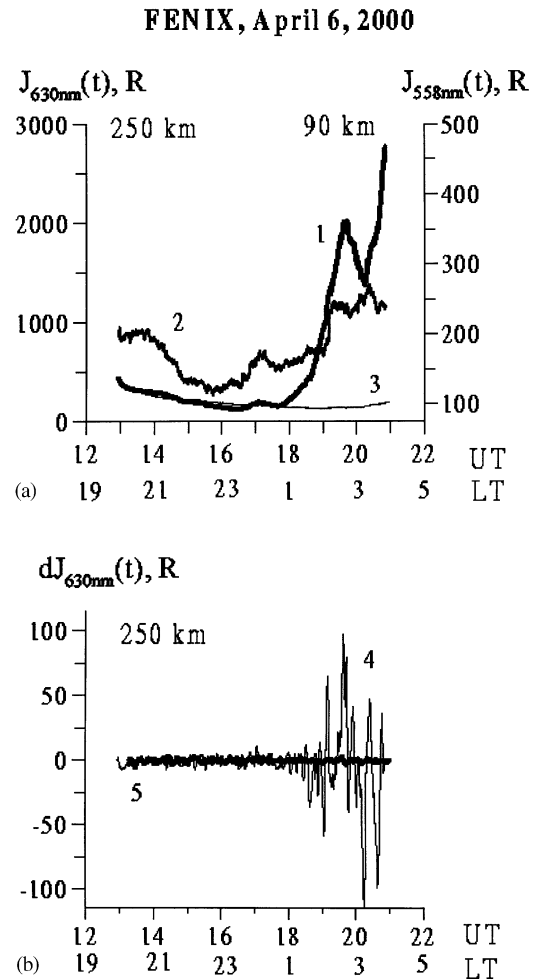


Fig. 5. Variations of the 630 nm,  $J_{630 \text{ nm}}(t)$  and 577.7 nm,  $J_{558 \text{ nm}}(t)$  emission rates (curve 1, 2, respectively) during magnetic storm of 6 April 2000 in universal (UT) and local (LT) times (a). Detrended variations of the 630 nm (curve 4),  $dJ_{630 \text{ nm}}(t)$  (b). For comparison, variations of the 630 nm emission rate (curve 3),  $J_{630 \text{ nm}}(t)$  corresponded to the magnetically quiet night of 5 April 2000 and detrended ones (curve 5),  $dJ_{630 \text{ nm}}(t)$  are plotted at panels (a) and (b), respectively. Data were obtained by FENIX instrument.

spheric airglow at estimated altitude of 94 km (Wiens et al., 1991; Aushev et al., 2000). The instrument comprises a conical mirror to receive the light from a full circle, a narrow band (0.27 nm halfwidth) interference filter centered at 867.6 nm, an imaging lens to focus the spectrum, and a CCD camera to record the spectrum. The emission rate and temperature observations have the precision of  $\pm 2\%$  and  $\pm 2\text{K}$ , respectively, when the exposure time is 5 min.

Variations of the  $O_2(867.6 \text{ nm})$  emission on 6 April 2000 are plotted by dots in Fig. 6a, and detrended variations are shown in Fig. 6b. The quadratic trend calculated by the least-squares technique (Fig. 6a, solid line) was subtracted

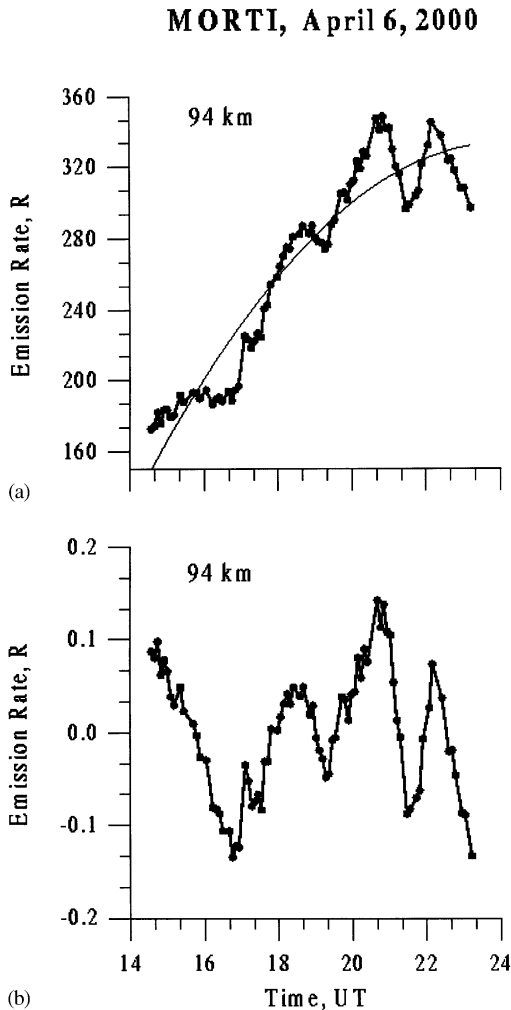


Fig. 6. Initial variations of emission rate (a) in the  $O_2$  (0-1) band (atmospheric airglow at estimated altitude of 94 km) and detrended ones (b) calculated from full images on the night of 6 April 2000. Data were obtained by MORTI instrument.

from the initial record to obtain the detrended variations. It is seen that large variations in the  $O_2$ (867.6 nm) emission were observed even before the time of the arrival of the solitary wave caused by the magnetic storm (this time is known from the GPS data).

The period of background variations was about 2 h, so the solitary wave excited by the magnetic storm can be distinguished because its period was about 1 h. In order to reduce the effect of 2-h background variations the high pass filter realized by the hour running window was applied to the record in Fig. 6b. Filtered variations of the  $O_2$ (867.6 nm) emission are plotted in Fig. 4e together with variations of TEC  $I(t)$  for the GPS station SELE. It is seen from Fig. 4e that there is a good correlation between the variations from the GPS and MORTI data. By comparing Fig. 4d and 4e,

it becomes evident that the phase delays between the variations of the GPS and optical data are different for Irkutsk and Almaty. This difference is explicable by the different altitudes of the nightglow emissions, and the different types of optical instruments.

### 5. Comparison of the auroral oval parameters with dynamic spectra of TEC variations and optical 630 nm emissions in the frequency range 0.4–4 mHz (2500–250 s periods)

It is known that an increase in auroral activity is accompanied by a change in the spectrum of ionospheric irregularities. For analyzing such changes, dynamic spectra of both GPS TEC and optical emissions from the FENIX instruments at Irkutsk were calculated.

#### 5.1. Dynamics of the auroral oval

To determine the position and dynamics of the auroral oval we used the data from the Space Environment Monitor (SEM) posted in the on-line mode at <http://sec.noaa.gov/pmap/pmapN.html>. The SEM includes a series of low-orbit (850 km) NOAA POES (Polar-Orbiting Operational Environmental Satellite) satellites with polar orbit (inclination  $98^\circ$ ). These satellites are constantly measuring electron and proton fluxes precipitating into the atmosphere. Based on using values of the flux power for a single satellite flight over the polar region (which takes about 25 min) and the database on more than 100,000 passes, the SEM technique makes it possible to estimate the integral energy released in this hemisphere and construct the position of the auroral oval for a given satellite pass.

Fig. 7 plots the variations of the power  $P(t)$  released by precipitating particles in the northern hemisphere (panel a) and of the latitudinal southern boundary  $\varphi_{\min}$  of the auroral oval (panel b) for the period of 5–7 April 2000. The position of the southern boundary of the auroral oval in the longitudinal sector  $80\text{--}100^\circ$  was determined from the particle flux power level  $0.1 \text{ erg/cm}^2 \text{ s}$  as accurate as  $1^\circ$ . The curves in the figures are smoothed by a polynomial of degree 10 (thick line).

On a quiet geomagnetic day, such as the day of 5 April 2000 preceding the storm, the integral energy  $P(t)$  that is identified in the northern hemisphere, varied from 3 GW to 15 W. The southern boundary  $\varphi_{\min}(t)$  of the auroral oval lay at about the latitudes of  $70\text{--}75^\circ\text{N}$  in the daytime and dropped to  $60\text{--}65^\circ\text{N}$  at night.

After the sudden storm commencement, SSC, at 16:40 UT on April 6, the auroral oval expanded rapidly southward. Within 20 min (16:40–17:00 UT) the southern boundary  $\varphi_{\min}(t)$  of the auroral oval moved abruptly from  $61^\circ\text{N}$  to  $57^\circ\text{N}$  (the displacement velocity was about 300–350 m/s). The oval's southern boundary remained at the latitudes  $56\text{--}57^\circ$  till about 19 UT. After that, as a consequence of a



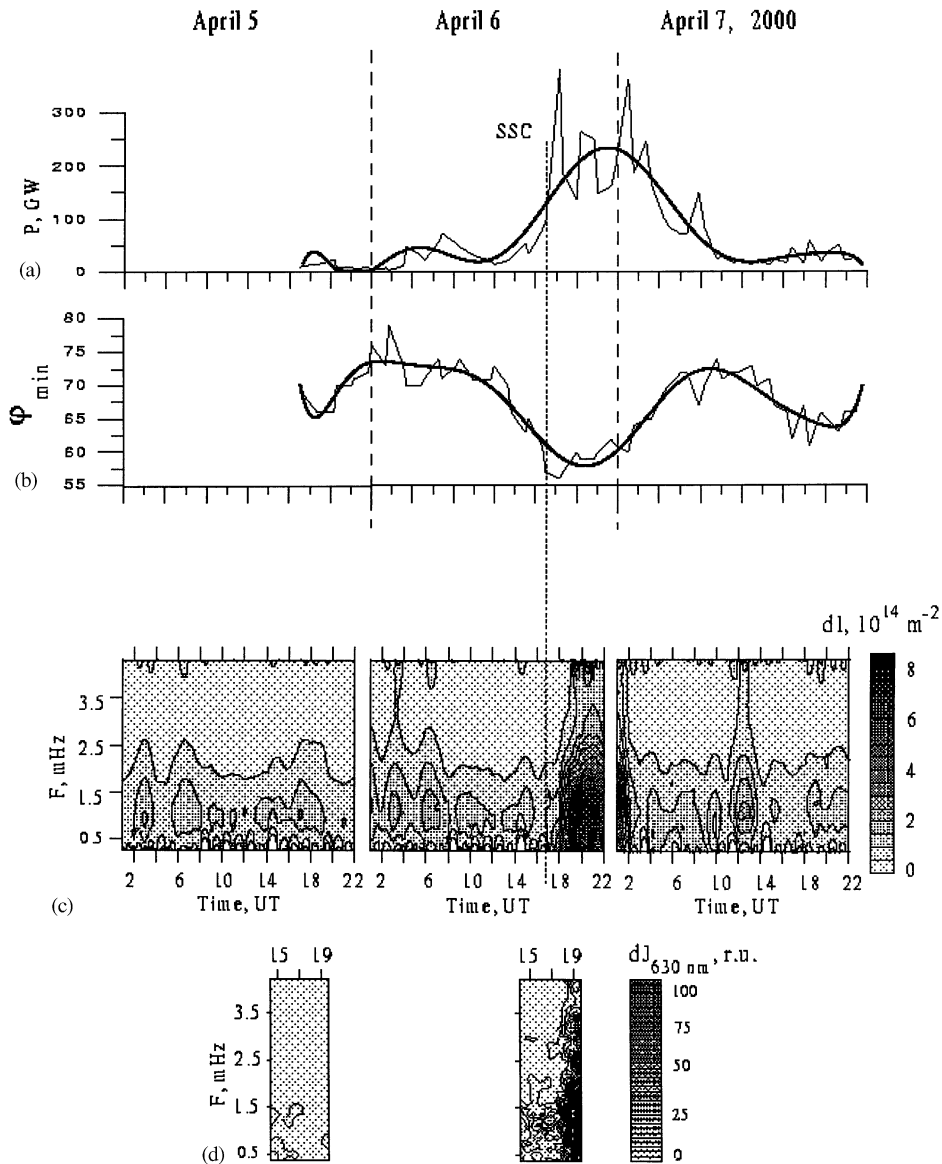


Fig. 7. A comparison of the auroral oval parameters with dynamic spectra of TEC variations and optical 630 nm emissions in the frequency range 0.4–4 mHz (250–2500 s periods): (a) the power  $P(t)$  released by precipitating particles in the northern hemisphere; (b) the latitudinal southern boundary  $\varphi_{\min}$  of the auroral oval (thin line). The curves obtained from data of the NOAA POES satellites <http://sec.noaa.gov/pmap/pmapN.html>. The curves in the panels a and b are smoothed by a polynomial of degree 10 (thick line). (c) the dynamic amplitude spectra of filtered variations  $dI(t)$  of TEC obtained through a spatial averaging of partial spectra over the latitude range  $40^{\circ}$ – $60^{\circ}$ N  $0^{\circ}$  –  $180^{\circ}$ E. (d) the dynamic spectra of filtered variations  $dJ_{630\text{ nm}}$  of optical emissions 630 nm (Fig. 5, curve 5) measured with the FENIX facility at observatory Irkutsk.

decrease in auroral activity and daybreak, the auroral oval receded northward. A subsequent development of the storm occurred when the Asian region was on the Earth’s day-side (20–06 UT); therefore, ionospheric effects of the storm were not as clearly pronounced.

### 5.2. Dynamic spectrum of TEC variations in the frequency range 0.4–4 mHz (2500–250 s periods)

Estimating the power spectrum of ionospheric irregularities using GPS data involves its own limitations

(Afraimovich et al., 2001). Unfortunately, for most stations of the global GPS network, the data are provided by the Internet at time intervals of 30 s, which bounds the TEC variation period below by about 1 min.

A calculation of a single spectrum of TEC variations involves using continuous series of  $dI(t)$  series of a duration of no less than 2.5 h, thus enabling us to obtain the number of counts equal to 256 that is convenient for the algorithm of fast Fourier transform (FFT) used in this study. To obtain a longer series of 512 counts requires a time interval no less than 5 h long, which is impracticable because of the limitations of the geometry of experiment with the GPS satellites. This bounds the range of periods analyzed by us above by about 120 min.

To exclude the variations of the regular ionosphere and LS TIDs-induced TEC variations, as well as trends introduced by the motion of the satellite, we employ the procedure of removing the linear trend with a selected time window of a duration of about 30–40 min. Thus the periods of TEC variations analyzed here are limited to the range 250–2500 s. A typical spatial size from 25 to 250 km (if the typical travel velocity of irregularities is taken to be 100 m/s), i.e. the range of medium and small scales (or, more exactly, the intermediate scale between the medium and small scales) corresponds to this range.

To improve the statistical validity of the data, we have used the method involving a global spatial averaging of disturbance spectra of the TEC (Afraimovich et al., 2001). As a consequence of the statistical independence of partial spectra, the signal/noise ratio, when the average spectrum is calculated, increases due to incoherent accumulation at least by a factor of  $\sqrt{n}$ , where  $n$  is the number of LOS.

The dynamic amplitude spectra in Fig. 7c were obtained through a spatial averaging of partial spectra over the latitude range 40–60°N 0–180°E. Gaps in the time interval 22–24 UT are caused by technical limitations of the analysis. As is evident from Fig. 7c, about 2 h after the SSC an abrupt increase in the intensity of TEC variations is observed, with a maximum value at 1 mHz frequency (a period of about 15 min) which exceeds no less than an order of magnitude the background value for the other time intervals used in the analysis.

### 5.3. Dynamic spectrum of optical emissions

The dynamic spectrum of variations of optical emissions (Fig. 7d) measured with the FENIX facility at observatory Irkutsk was obtained in a similar way. Optical observations were made at night only; therefore, the intervals of analysis of the dynamic spectrum of the emissions is significantly shorter than that for the TEC.

The enhancement of the fluctuation intensity of optical 630 nm emission in the frequency range 1–2 mHz (1000–500 s periods) after 19:00 UT is illustrated by Fig. 5b. Fig. 7d presents a corresponding dynamic spectrum. As is evident from Fig. 7, the intensity enhancement

of oscillations with periods of 500–1000 s for both optical emissions and TEC variations is almost time-coincident with the abrupt increase in integral energy released by precipitating particles in the northern hemisphere, and with the maximum displacement of the southern boundary of the auroral oval (up to the latitude 56° near Irkutsk).

## 6. Discussion

It is well known that major geomagnetic storms cause substantial, varied changes in the upper atmosphere. Investigations of ionospheric storms were addressed by a large number of publications, both experimental and theoretical (see, e.g., reviews by Buonsanto, 1999; Danilov and Lastovicka, 2001). Nevertheless, it is not yet possible to sufficiently reliably forecast the response of the upper atmosphere to the geomagnetic storm. This is caused by the complexity and uniqueness of each particular geomagnetic storm. Furthermore, although there is an immense experimental data set, these data are often heterogeneous, incomplete and conflicting. For that reason, it is extremely important to have reliable experimental data on several measured parameters for every major magnetic storm.

This experimental study is based on TEC variations with wide coverage in longitude and latitude, obtained using the data from the GPS system, and on observations of optical emissions made near Irkutsk and Almaty. A number of other data were also used: the position of the auroral oval, geomagnetic indices, TEC data, and the data from the vertical-incidence ionospheric sounding station at Almaty. Let us consider these data within the context of existing concepts of the development of the geomagnetic storm (without seeking complete explanation).

1–1.5 h after the SSC (i.e. at about 18 UT) there occurs a peak increase in energy released by energetic particle fluxes into the earth's atmosphere in the northern hemisphere, as high as a level of 380 GW (Fig. 7a). The same period (17:30–18:00 UT) shows an enhancement of the auroral electrojet intensity estimated from the AE-index which reaches 1500 nT (<http://swdcd.db.kugi.kuotou.jp/el/q/Rae.000406.html>). The dissipation of precipitating particle energy (at 100–150 km altitudes) and an enhancement of electrojets flowing at ionospheric E-layer heights (90–120 km) are accompanied by a heating of the neutral atmosphere. Since the heating has an impulsive character, a large-scale acoustic-gravity wave is generated.

This wave is clearly identified in data on TEC variations from subauroral to low latitudes (Figs. 3 and 4). The wave front with an extent in longitude from Zvenigorod (36.8°E) to Yakutsk (129.6°E), i.e. of 5000 km as a minimum, moves in a southward direction with the velocity of about 200 m/s. This is accompanied by a spreading of the LS TIDs and a decrease in the TEC variation amplitude (at the Yakutsk

latitude,  $A_{\min}$  reaches  $-4.5$  TECU, and at the Almaty latitude  $A_{\min}$  reaches  $-0.6$  TECU).

The decrease of the TEC can be caused by two factors: a change in the composition of the neutral atmosphere (or, more exactly, by a decrease of the ratio  $O/N_2 + O_2$ ), and by an increase of the recombination coefficient caused by a rise of temperature (Buonsanto, 1999). This is suggested by the anti-correlation, obtained at Irkutsk, between the 630 nm emission intensity at the F2-layer height and the TEC, the main contribution to which is made by the F2-layer (Fig. 4d). It is known (Wickwar et al., 1974) that the escape rate of electrons and the increase of the 630 nm emission intensity are determined by the same reactions which govern the population and depletion of the  $^1D$  state of atomic oxygen:

- (1) ion–molecular recombination:  $-O^+ + O_2 \rightarrow O_2^+ + O$ ;
- (2) dissociative recombination:  $-O_2^+ + e \rightarrow O(^1D) + O$ .

Conceivably LS AGWs transport from high latitudes the region with increased temperature and increased density of  $O_2$ , which leads to a decrease of the TEC and an increase of the 630 nm line emission intensity.

On the other hand, for a certain range of mid-latitudes lying southward of the subauroral zone, except for disturbances in the form of LS TIDs, in the case of major geomagnetic storms, we should expect disturbances associated with the equatorward displacement of main structural elements of the subauroral and auroral ionosphere, such as the auroral oval, the main ionospheric trough (MIT), and the plasmopause boundary projection.

As is evident from Fig. 7b, during 17–21 UT the southern boundary of the auroral oval reached  $56$ – $58^\circ N$ . Considering that the MIT width in disturbed conditions can reach about  $5$ – $6^\circ$ , it may be anticipated that Irkutsk is in the region of the southern boundary of the MIT. During periods of great geomagnetic activity, the plasmopause boundary may approach extreme values of  $L$  in the range of  $1.7$ – $2.5$  (Khorosheva, 1987). For Irkutsk, the value of  $L$  is on the order of  $2$ . The plasmopause projection in the night-time F-region corresponds to the boundary of the main ionospheric trough. These facts suggest that in the course of the magnetic storm considered, elements of the subauroral and even auroral ionosphere were observed at latitudes of Irkutsk. Unfortunately, it is not possible to determine the MIT boundaries using the data from a relatively sparse Asian part of the global GPS stations network.

It is customary to associate the occurrence of stable auroral red (SAR) arcs with the plasmopause region (Rees and Roble, 1975; Rassoul et al., 1993). For mid-latitude auroras with 630 nm emission predominating, Rassoul et al. (1993) point out the plasmopause as the region of localization. However, SAR-arcs are usually observed during recovery phases of magnetic storms. Optical observational data obtained at Irkutsk for the next night of 7 April 2000 (recovery phase of the magnetic storm) reveal disturbances in 630 nm emission

for the time interval  $\sim 15$ – $17$  UT with intensities as high as 500 RI which may be tentatively interpreted as a SAR-arc. SAR-arcs in the Asian region have not yet been carried out for major magnetic storms.

Rassoul et al. (1993) point out one further type of mid-latitude auroras (type d), with 630 nm emission predominating, and with its localization also in the plasmopause region but differing by the energy of exciting particles and caused by an increase of thermal fluxes as a result of the ring current enhancement during the development of the geomagnetic storm.

The simultaneous propagation of LS TIDs and the possible localization of the plasmopause projection near the Irkutsk latitude makes an unambiguous interpretation of the behavior of recorded emissions difficult (Mikhalev, 1997). It seems likely that the overall increase in the 630 nm emission intensity (Fig. 5a) is caused by the heating of the ionospheric F-region induced by the displacement of auroral structures to mid-latitudes, and the local increase of  $J_{630\text{ nm}}$  is associated with LS TIDs.

The simultaneous enhancement of short-period variations of the TEC and  $J_{630\text{ nm}}$  in the range of 250–2500 s periods (Fig. 7c and d) was obtained for the first time, as far as our knowledge goes. This enhancement is possibly associated with energetic particle precipitation (Aarons and Lin, 1999), which is characteristic for the subauroral and auroral ionosphere and lends support to the assumptions made above. The enhancement of short-period variations of the TEC and  $J_{630\text{ nm}}$  correlates quite well with the largest displacement of the auroral oval into mid-latitudes (Fig. 7b). This is consistent with results obtained using the data from the global GPS network by Pi et al. (1997). They established that enhance short-period TEC disturbances propagate in the space in accordance with the movement of the auroral oval.

Energetic particle precipitation can be used to interpret the enhancement of the signal in the spectral range 360–410 nm after 17.00 UT as the appearance of  $N_2^+$  (ING) emissions with 391.4 nm wavelength which usually occur in polar auroras as a result of the ionization of molecular nitrogen by precipitating electrons or precipitation of energetic atoms or ions (Ishimoto et al., 1986; Tinsley et al., 1984).

For the storm under investigation at latitudes above  $50^\circ N$ , experimental results show an overlapping of two processes. One is associated with the displacement of auroral structural elements to low-latitudes. This manifests itself in total increase of atomic oxygen 630 nm optical emission, the appearance of auroral emission with 391.4 nm wavelength and an enhancement of short-period variations of both TEC and  $J_{630\text{ nm}}$ . The other process involves the propagation of LS TIDs having its origin in high altitudes. Auroral structures do, of course, not reach the stations located below  $50^\circ N$ , and there are virtually no intense short-period variations (Fig. 4). On the other hand, LS TIDs are relatively clearly distinguished, although their amplitude is smaller.

## 7. Conclusion

In the course of the magnetic storm of 6 April 2000, two types of disturbances were observed. The first one has features of a solitary wave with a period of about 1 h, and was interpreted as an LS TID originating in the polar latitudes. The second one included short-period variations probably related to the particle precipitation. An analysis of the data has shown that being originated the auroral disturbance induced LS solitary wave with a period of about 1 h and the front width no less 5000 km traveled equatorward to a distance no less than 1000 km with the average velocity of about 200 m/s. The TEC disturbance, showing mainly a decrease of the electron content in the vicinity of the F2-layer maximum, correlates with an increase of the emission rate in the optical band, with the temporal shift being different for different ionospheric altitudes.

Thus, main results of this study may be summarized as follows:

1. Experimental data of optical observations and on TEC variations have been obtained for the first time in the Asian region for a unique magnetic storm of 6 April 2000.

2. For the first time, a correlation was shown to exist between short-period TEC variations and optical emissions  $J_{630\text{ nm}}$  the range of 250–2500 s periods.

3. Effects in the upper atmosphere associated with the displacement of large-scale ionospheric structures (auroral oval) into mid-latitudes and effects of LS TIDs have, for the first time, been analyzed and, to a certain extent, separated.

4. Other available experimental data have been summarized and systematized, which will be very useful for a further analysis of this storm.

## Acknowledgements

We are grateful to E.A. Ponomarev and A.V. Tashchilin for their encouraging interest in this study, and for active discussions. Finally, the authors wish to thank the referees for valuable suggestions which greatly improved the presentation of this paper. This work was done with support of INTAS Grant no. 99-1186, the Russian foundation for Basic Research (Grants 99-05-64753 and 00-05-72026) and RFBR grant of leading scientific schools of the Russian Federation no. 00-15-98509.

## References

Aarons, J., Lin, B., 1999. Development of high latitude phase fluctuations during the January 10, April 10–11 and May, 15, 1997 magnetic storms. *Journal of Atmospheric and Solar-Terrestrial Physics* 61, 309–327.

Afraimovich, E.L., Palamarchouk, K.S., Perevalova, N.P., 1998. GPS radio interferometry of traveling ionospheric disturbances. *Journal of Atmospheric and Solar-Terrestrial Physics* 60, 1205–1223.

Afraimovich, E.L., Kosogorov, E.A., Lenovich, L.A., Palamarchuk, K.S., Perevalova, N.P., Pirog, O.M., 2000. Determining parameters of large-scale traveling ionospheric disturbances of auroral origin using GPS-arrays. *Journal of Atmospheric and Solar-Terrestrial Physics* 62, 553–565.

Afraimovich, E.L., Kosogorov, E.A., Lesyuta, O.S., Ushakov, I.I., Yakovets, A.F., 2001. Geomagnetic control of the spectrum of traveling ionospheric disturbances based on data from a global GPS network. *Annales Geophysicae* 19, 723–731.

Aushev, V.M., Pogoreltsev, A.I., Vodyannikov, V.V., Wiens, R.H., Shepherd, G.G., 2000. Results of the airglow and temperature observations by MORTI at the Almaty site (43.05°N, 76.97°E). *Physics and Chemistry of the Earth (B)* 25 (56), 409–415.

Balthazor, R.L., Moffett, G.G., 1999. Morphology of large-scale traveling atmospheric disturbances in the polar thermosphere. *Journal of Geophysical Research* 104 (A1), 15–24.

Buonsanto, M.J., 1999. Ionospheric storms—a review. *Space Science Reviews* 88, 563–601.

Chapman, S., 1957. The aurora in middle and low latitude. *Nature* 179, 7–11.

Danilov, A.D., Lastovicka, J., 2001. Effects of geomagnetic storms on the ionosphere and atmosphere. *International Journal of Geomagnetism and Aeronomy* 2 (3), <http://ijga.wdcb.ru/v02/gai99312/gai99312.htm>.

Hajkowicz, L.A., Hunsucker, R.D., 1987. A simultaneous observation of large-scale periodic TIDs in both hemispheres following an onset of auroral disturbances. *Planetary Space Science* 35 (6), 785–791.

Ho, C.M., Iijima, B.A., Lindqwister, X.P., Mannucci, A.J., Sparks, L., Reyes, M.J., Wilson, B.D., 1998. Ionospheric total electron content perturbations monitored by the GPS global network during two northern hemisphere winter storms. *Journal of Geophysical Research* 103, 26,409–26,420.

Hocke, K., Schlegel, K., 1996. A review of atmospheric gravity waves and traveling ionospheric disturbances: 1982–1995. *Annales Geophysicae* 14, 917–940.

Hofmann-Wellenhof, B., Lichtenegger, H., Collins, J., 1992. *Global Positioning System: Theory and Practice*. Springer, Wien, New York, p. 327.

Hunsucker, R.D., 1982. Atmospheric gravity waves generated in the high-latitude ionosphere. A review. *Review of Geophysics* 20, 293–315.

Ishimoto, M., Torr, M.R., Richards, P.G., Torr, D.G., 1986. The role of energetic O<sup>+</sup> precipitation in a mid-latitude aurora. *Journal of Geophysical Research* 91, 5793–5802.

Khorosheva, O.V., 1987. On relations auroral forms and low-latitudes red arcs. *Geomagnetizm i Aeronomy* 27, 804–811 (in Russian).

Klobuchar, J.A., 1986. Ionospheric time-delay algorithm for single-frequency GPS users. *Transactions on Aerospace and Electronics System* 23 (3), 325–331.

Maeda, S., Handa, S., 1980. Transmission of large-scale TIDs in the ionospheric F2-region. *Journal of Atmospheric and Terrestrial Physics* 42, 853–859.

Mannucci, A.J., Ho, C.M., Lindqwister, U.J., Runge, T.F., Wilson, B.D., Yuan, D.N., 1998. A global mapping technique for GPS-driven ionospheric TEC measurements. *Radio Science* 33, 565–582.

Mikhalev, A.V., 1997. Photometric observation of midlatitude auroras over South-East Siberia. Eighth Scientific Assembly of IAGA with ICMA and STP Symposia, Uppsala, August 4–15 p. 161, Abstracts.

- Misawa, K., Takeuchi, I., Aoyama, I., 1984. Apparent progression of intensity variations of the oxygen red line. *Journal of Atmospheric and Terrestrial Physics* 46 (1), 39–46.
- Pi, X., Mannucci, A.J., Lindqwister, U.J., Ho, C.M., 1997. Monitoring of global ionospheric irregularities using the Worldwide GPS network. *Geophysical Research Letters* 24, 2283–2286.
- Prolss, G.W., Brace, L.H., Mayr, H.G., Caringan, G.R., Killeen, T.L., Klobuchar, J.A., 1991. Ionospheric storm effects at subauroral latitudes: a case study. *Journal of Geophysical Research* 96 (A2), 1275–1288.
- Rassoul, H.K., Rohrbaugh, R.P., Tinsley, B.A., Slater, D.W., 1993. Spectrometric and photometric observation of low-latitude aurora. *Journal of Geophysical Research* 98 (A5), 7695–7709.
- Rees, M.H., Roble, R.G., 1975. Observations and theory of the formation of stable auroral red arcs. *Review of Geophysical Space Physics* 13 (1), 201–242.
- Sahal, Y., Bittencourt, J.A., Takahasili, H., Teixeira, N.R., Sobral, J.H., Tinsley, B.A., Rohrbaugh, R.P., 1988. Multispectral optical observations of ionospheric F-region storm effects at low latitude. *Planetary Space Science* 36 (4), 371–381.
- Tinsley, B.A., 1979. Energetic neutral atom precipitation during magnetic storm: optical emission, ionization, and energy deposition at low and middle latitudes. *Journal of Geophysical Research* 84, 1855–1864.
- Tinsley, B.A., Rohrbaugh, R.P., Rassoul, H., Barker, E.S., Cochran, A.L., Cochran, W.D., Wills, B.J., Wills, D.W., Slater, D., 1984. Spectral characteristics of two types of low latitude aurora. *Geophysical Research Letters* 11 (6), 572–575.
- Torr, M.R., Torr, D.G., 1984. Energetic oxygen in mid-latitude aurora. *Journal of Geophysical Research* 89, 5547–5553.
- Whalen, J.A., 1987. Daytime F-layer trough observed on a macroscopic scale. *Journal of Geophysical Research* 92, 2571–2576.
- Wickwar, V.B., Cogger, L.L., Carlson, H.C., 1974. The 6300A O(<sup>1</sup>D) airglow and dissociative recombination. *Planetary Space Science* 22 (5), 709–724.
- Wiens, R.H., Zhang, S.P., Peterson, R.N., Shepherd, G.G., 1991. MORTI: a mesopause oxygen rotational temperature imager. *Planetary Space Science* 39, 1363–1375.
- Wilson, B.D., Mannucci, A.J., Edwards, C.D., 1995. Subdaily northern hemisphere maps using the IGS GPS network. *Radio Science* 30, 639–648.
- Wrenn, G.L., Rodger, A.S., Rishbeth, H., 1987. Geomagnetic storm in the Antarctic F-region. *Journal of Atmospheric and Terrestrial Physics* 49 (9), 901–913.
- Yeh, K.C., Ma, H., Lin, K.H., Conkright, R.O., 1994. Global ionospheric effects of the October 1989 geomagnetic storm. *Journal of Geophysical Research* 99 (A4), 6201–6218.